Positron annihilation lifetime spectroscopy using fast scintillators and digital electronics

M. Fang *, N. Bartholomew, A. Di Fulvio

Department of Nuclear, Plasma, and Radiological Engineering, University of Illinois, Urbana-Champaign, 104 South Wright Street, Urbana, IL 61801, United States

Keywords:
Positron lifetime
Organic scintillator
Digitizer
CFD

A B S T R A C T

Positron Annihilation Lifetime Spectroscopy (PALS) is a non-destructive radiological technique widely used in material science studies. PALS typically relies on an analog coincidence measurement setup and allows the estimate of the positron lifetime in a material sample under investigation. The positron trapping at vacancies in the material results in an increased positron lifetime. In this work, we have developed and optimized a PALS experimental setup using organic scintillators, fast digitizers, and advanced pulse processing algorithms. We tested three pairs of different organic scintillators: EJ-309 liquid, EJ-276 newly developed plastic, and BC-418 plastic, and optimized the data processing parameters for each pair separately. Our high-throughput data analysis method is based on single-pulse interpolation and a constant fraction discrimination (CFD) algorithm. The setup based on the BC-418 detector achieved the best time resolution of 198.3 ± 0.8 ps. We used such optimized setup to analyze two single-crystal quartz samples and found lifetimes of 161 ± 4 ps, 343 ± 12 ps and 1.34 ± 0.05 ns, in good agreement with the characteristic time constants of this material. The proposed experimental set up achieves a time resolution comparable to the minimum positron lifetime in quartz, which makes it possible to accurately characterize material vacancies by discriminating between the lifetimes of either the spin singlet or triplet states of positronium. The optimized data processing algorithms are relevant to all the applications where fast timing is important, such as nuclear medicine and radiation imaging.

1. Introduction

PALS is a well-established non-destructive technique used to study defects and vacancies in a variety of different materials. Different positron sources may be used, such as radionuclides (e.g., ^{22}Na), nuclear reactors, and electron accelerators. Apart from direct annihilation with the electrons in material, thermalized positrons may bind with electrons in the material and form two types of positronium: para-positronium (p-Ps) with spin 0 and ortho-positronium (o-Ps) with spin 1. The p-Ps decays by emitting two 511-keV annihilation photons, while the o-Ps mainly decays via the ''pick-off'' process, where the positron annihilates with an electron with opposed spin in the surrounding material, rather than with the electron that is part of the o-Ps. Following this process, two 511-keV annihilation photons are created [1]. The elapsed time between the initial production of the positron and the detection of the annihilation photon is therefore a measurement of the positron lifetime in the material under investigation.

The positron lifetime depends on the material structure. In vacuum, the lifetimes of p-Ps and o-Ps are 125 ps and 142 ns, respectively [2]. The p-Ps lifetime can be affected by the material because the Coulomb interaction between the p-Ps and material electrons changes the distance between the positron and electron in p-Ps [3]. The o-Ps lifetime in a material is reduced drastically due to the ''pick-off'' process. If the material contains voids, vacancies or dislocations, the o-Ps can be trapped and the lifetime will be increased compared to the lifetime in a defect-free material. Thus, the positronium ion, especially o-Ps can be used as a probe to investigate the material properties, such as defect density in metals [4] and pore characteristics in porous materials [5]. We may also use the PALS to differentiate between different lattice structures of the same material since the positron lifetime depends on the interaction between the positron and lattice [6].

Time resolution of the measurement system is crucial to perform an accurate measurement of positron lifetime. Hodges and colleagues [7] set up a system with 330 ps time resolution but they were unable to resolve the p-Ps component from the spectra. Haruo and Toshio [3] achieved 160 ps time resolution with four BaF_2 scintillators. However, severe piled-up phenomena will occur at count rate higher than 360 kcps [8], which affect the shape of the pulse and thus the zero-crossing time. In this work, we compared the timing resolution of PALS using three different organic scintillators and chose the one with the best timing resolution to perform PALS measurements of single-crystal quartz. In recent years, digital electronics, such as digital oscilloscopes [9] and fast digitizers [10], are replacing traditional analog timing modules in

* Corresponding author.
E-mail address: mingf2@illinois.edu (M. Fang).

Table 1
Properties of BC-418, EJ-309 and EJ-276 detectors.

Scintillator	Ratio H:C	Base (cm)	Top (cm)	Height (cm)	Density (g/cm^3)	PMT	PMT response time (ns)	Pulse shape discrimination
BC-418	1.100	3.18	1.27	1.27	1.032	R329-02 by Hamamatsu Photonics	2.6	Not capable
EJ-309	1.248	5.08	5.08	5.08	0.959	9214B by Electron Tubes	2	Capable
EJ-276	0.927	5.08	5.08	5.08	1.096	9214B by Electron Tubes	2	Capable

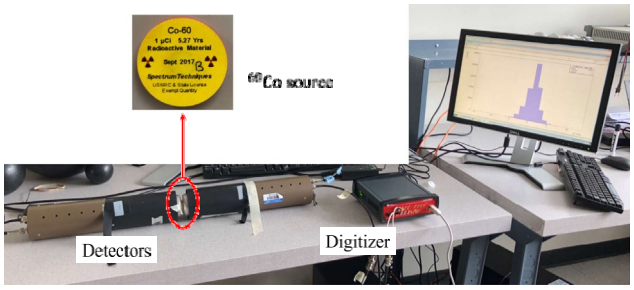

Fig. 1. Detector time resolution measurement setup.

PALS experiments. Digital signal processing therefore becomes another important factor that can improve the time resolution. We have developed a timing algorithm based on pulse interpolation and optimized the processing parameters for three different organic scintillators.

2. Methods

We measured the time resolution of three different pairs of scintillators and selected the scintillators that exhibited the best time resolution to then perform the PALS experiment. We performed a PALS measurement using a ^{22}Na source and measured the distribution of the differences of arrival times between the 1.27 MeV ^{22}Na decay gamma ray and the 511 keV annihilation gamma ray.

2.1. Time resolution measurement

We used the experimental setup shown in Fig. 1 for timing resolution measurement. We performed three measurements with two plastic BC-418, two liquid EJ-309, and two plastic EJ-276 scintillators. Table 1 shows the properties of these scintillators and photomultiplier tubes (PMT) that were used with them. The use of a pair of fast PMTs of the same model makes their time contribution to the differential measurement of time resolution negligible.

The time resolution of each scintillator pair was estimated as the full-width-at-half-maximum (FWHM) of the distribution of differences of arrival times of two events occurring in coincidence. In this case, the 1.17 MeV and 1.33 MeV gamma rays emitted in cascade by a ^{60}Co source are used as reference. A 1 μCi ^{60}Co disk source was placed between the two scintillators under investigation in a sandwich configuration (Fig. 1). Approximately 500k counts in coincidence were collected during each measurement. Detected pulses were digitized by the 14-bit 500 MS/s digitizer DT5730 by CAEN Technologies and acquired as full waveforms using the acquisition software CoMPASS [11] with a 200-ns coincidence window. The detectors were powered by the Desktop HV Power Supply Module DT5533EN by CAEN Technologies.

We applied the timing algorithm described in Section 2.2 and performed a Gaussian fitting to obtain the standard deviation □ of the distribution of the intervals between the detection of the 1.17 MeV and 1.33 MeV gamma rays and the full width at half maximum (FWHM =

2.2. Timing algorithm

First, we interpolated the digitized pulses because signal information may be partially lost due to insufficient sampling rates. Multiple functional forms have been used to approximate scintillation pulses, such as those based on double-exponential functions that describe the different time constants of scintillation phenomena [12,13]. However, for such models to be accurate, a deep knowledge of scintillation molecular processes is needed. Here we adopted a different approach based on the Nyquist sampling theorem. This approach does not introduce biases (e.g., from neglecting a scintillation time constant) when applied to different detectors. The input signal can be reconstructed by convolving the samples with the *sinc* function if the Nyquist condition is satisfied [14].

$$□(□) = \mathrm{sinc}(□) * □_□(□) = \sum_{□=-}^{+∞} □_□(□)\,\mathrm{sinc}\left(\frac{□ - □□□}{□}\right) \quad (1)$$

Here $□_□(□)$ is the □th sample, $□ = 1/□□$ is the sampling rate, and thenormalized *sinc* function is defined as

$$\mathrm{sinc}(□) = \frac{\sin(□□)}{□□} \quad (2)$$

Dividing the time interval between sample □ and sample □ + 1 into □ even parts, the □th interpolated value between them is given by

$$□(□, □) = \sum_{□=-∞}^{∞} □_□(□ - □)\,\mathrm{sinc}(□ + □/□) \quad (3)$$

However, Eq. (3) is not suitable for practical use since the index of summation extends to infinity and a terminated *sinc* function is used as the convolution kernel [15], as in Eqs. ((4), (5))

$$□(□, □) = \sum_{□=-∞}^{∞} □_□(□ - □)\,\mathrm{tsinc}(□□ + □) \quad (4)$$

$$\mathrm{tsinc}(□) = \mathrm{sinc}(□/□)\exp(-(□/□)^2) \quad (5)$$

Here □ is a constant and the Gaussian term quickly drops to 0 as □ increases. Thus, the terms in Eq. (4) for sufficiently large values of □ can be safely ignored and Eq. (4) reduces to a finite sum [15]

$$□(□, □) = \sum_{□=0}^{□} □_□(□ - □)\,\mathrm{tsinc}(□□ + □) + □_□(□ + 1 + □)\,\mathrm{tsinc}((□ + 1)□ - □) \quad (6)$$

where □ is the width of interpolation window.

Afterwards, we applied a digital version of the constant-fraction discrimination (CFD) algorithm [16] to each interpolated pulse and obtained the zero-crossing bipolar CFD(i) signal.

$$\mathrm{CFD}(□) = □ \times □(□) - □(□ - □) \quad (7)$$

In Eq. (7), □(□) is the value of interpolated pulse at index □, □ and □ aretwo constants. □ is between 0 and 1, and □ is a delay time, which is usually comparable to the pulse rise time. □ and □ will be determined later by optimizing the detector time resolution. The zero-crossing point of CFD(i) is defined as the time stamp.

We have implemented the above-mentioned algorithms in a ROOT-based pulse-processing program.[1] This software allows us to process 1E6 pulses in approximately 10 s using Intel Core i9-7920X @ 2.90 GHz.

$2\sqrt{2\ln 2}$).

[1] https://github.com/fm140905/coincidence.git.

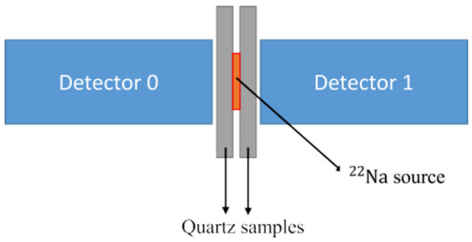

Fig. 2. Schematic diagram of the PALS measurement setup using two BC-418 detectors (not to scale).

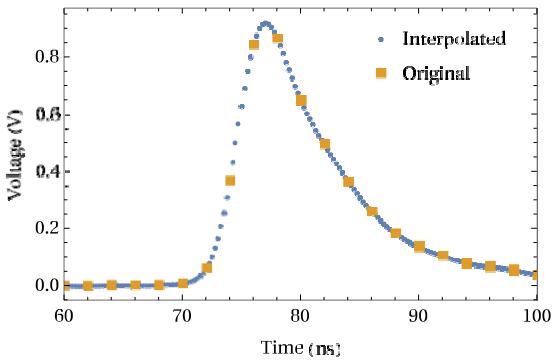

Fig. 3. An example pulse before and after interpolation obtained from BC-418 scintillators.

Table 2
Comparison of detector time resolutions.

Detector	□ (ns)	□	□ (ps)	FWHM (ps)
BC-418	4	0.4	84.2 ± 0.3	198.3 ± 0.8
EJ-309	10	0.2	172.5 ± 0.3	406.3 ± 0.8
EJ-276	6	0.05	215.1 ± 0.3	507.4 ± 0.7

2.3. PALS measurement

The PALS experimental setup is shown in Fig. 2. A 10 μCi (1-July-2004) ^{22}Na source was placed in sandwich geometry between two identical single-crystal quartz samples (10 mm ×10 mm ×1 mm each). ^{22}Na was sealed between two identical Kapton foils. ^{22}Na emits a positron and the daughter nucleus de-excites in about 3 ps by emitting a 1.27 MeV gamma ray. The detection of the 1.27 MeV gamma ray can be used to probe the creation of the positron. The quartz samples were purchased from MTI Corporation. The two scintillation detectors were placed back to back to achieve the highest detection efficiency. By proper energy gating, detector 0 and detector 1 detected the 1.27 MeV and 511 keV gamma rays, respectively. We acquired pulses in coincidence, within a 200-ns time window.

We applied the timing algorithm and plotted the positron annihilation lifetime spectra. The PALS spectra are usually resolved into three components. The first component results from the decay of p-Ps, the second one from the mixture of decays of o-Ps and free positron, and the third one is due to the delayed decay of o-Ps trapped in defects [6]. The PALS spectrum can therefore be modeled as the convolution of exponential decay function and detector time resolution function, as shown in Eq. (8),

$$\square(\square) = \sum_{\square=} \frac{1}{\square_{\square}} e^{-\frac{\square}{\square_{\square}}} * \frac{1}{\sqrt{2\pi\square^2}} e^{-\frac{\square^2}{2\square^2}} + \sum_{\square=1}^{3} \frac{\square_{\square}}{2\square_{\square}} e^{\frac{\square^2}{2\square_{\square}^2} - \frac{\square}{\square_{\square}}} \left[1 - \operatorname{erf}\left(\frac{\square^2 - \square}{\sqrt{2}\square}\right)\right]$$

3. Results

3.1. Detector timing resolution

Fig. 3 shows the comparison between an interpolated signal pulse and the original one. The true peak of the original pulse is not captured and only a few sampling points are recorded on the rising edge due to insufficient sampling frequency. Interpolation helps in the characterization of the rising edge by adding more sampling points and gives a more accurate estimate of the true peak based on model assumptions. Since CFD relies on the identification of the time corresponding to the maximum value and a fraction of it, the time stamp would be more accurate if we perform CFD after interpolation. As a result, the time resolution would be improved since it is the spread of the arrival times.

Fig. 4 shows the time interval distribution before and after interpolation for signals measured with BC-418 scintillators. In Fig. 4(a), we performed Gaussian fitting of the spectra to calculate the FWHM and found that interpolation improved the time resolution by approximately 33 ps. The spectra are not centered at 0 because of the inherent asymmetry of acquisition stages, such as slightly different cable lengths.

The interpolation algorithm also helps to reduce the skewness of the time interval histogram. With □ fixed, an overly small □ usually leads to a skewed histogram because the zero-crossing point lies near the beginning of the rising edge and linear interpolation fails in this region, as shown in Fig. 3. Fig. 4(b) shows two time interval distributions before and after interpolation, with □ = 0.2 and □ = 6 ns. After interpolation, the time interval histogram is more symmetrical because interpolation reduces the uncertainty at the beginning of the rising edge by adding more points.

The FWHM of the time interval distribution depends on the CFD parameters □ and □. Figs. 5(a), 5(b), 5(c) illustrate the optimization of □ and □ for each scintillator pair. We increased □ in steps of 2 ns and for each □ we decreased □ from 1 until severe artifacts appeared on the spectrum. For each combination of □ and □ we fitted a Gaussianto the spectrum and calculate the FWHM. Fig. 6 shows the best time resolution of each scintillator pair. Time resolutions of EJ-276 and EJ-309 are close to each other and BC-418 exhibits the best time resolution. The minimum 125.7 ps □ (296.0 ps FWHM) is obtained withBC-418 scintillators at □ = 0.4 and □ = 4 ns.

We can further reduce the FWHM by rejecting the low energy pulses. These pulses have small amplitudes and the sampling values could be easily affected by the noise, which leads to large errors of the time stamps and creates a long tail in Fig. 4. After rejecting pulses with deposited energy less than 600 keVee, the minimum FWHM and optimized parameters of each detector pair are summarized in Table 2. The BC-418 scintillators yielded the best time resolution and were used in the PALS experiment.

3.2. Positron lifetime in single-crystal quartz

Fig. 7 shows the comparison of the positron lifetime spectrum in quartz and the distribution of arrival times obtained using the ^{60}Co. The positron lifetime spectrum shows a longer tail due to longer lifetime, as expected.

We collected 1.1 million counts with a count rate of approximately 4 cps. We fitted Eq. (8) to the positron annihilation lifetime spectrum using the LT10 program [17], which is the one of the most widely used PALS analysis software. The result is shown in Fig. 8. The intensities and lifetimes are shown in Table 3. Three lifetime components were successfully resolved from the spectrum. The lifetimes □$_1$, □$_2$ and □$_3$ are 161 ps, 343 ps and 1.34 ns, respectively, and are consistent with the reported values of 156 ps [3], 329 ps [6] and 1.50 ns [6,18]. The relative standard error of □$_1$, □$_2$, and □$_3$ is 2.5%, 3.5%, and 3.8%. The latter component results from o-Ps trapping and subsequent annihilation in

$$\mathrm{erfc}(\ldots 2 \ldots) \quad (8)$$

voids, vacancies and dislocations. This component is hard to detect because of the high purity and high internal crystalline perfection of –

where □□ and □□ are the lifetime and intensity of the □th component, □
represents the detector time resolution, i.e., FWHM/2 $\sqrt{2 \ln 2}$.

the single-crystal quartz samples, where defects such as micro-bubbles and cracks are not formed during the manufacturing process.

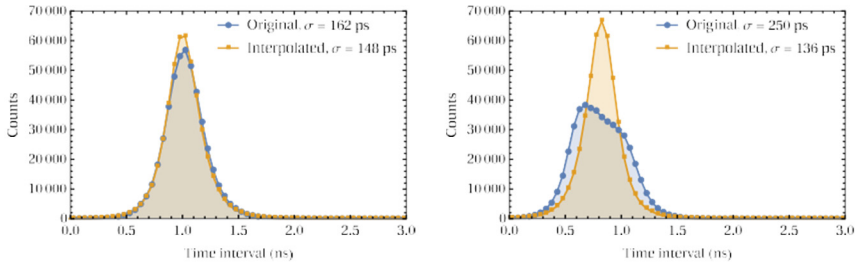

(a) F = 0.75, Δ = 6 ns (b) F = 0.2, Δ = 6 ns

Fig. 4. The time interval distribution before interpolation and after interpolation. Measured with BC-418 detectors.

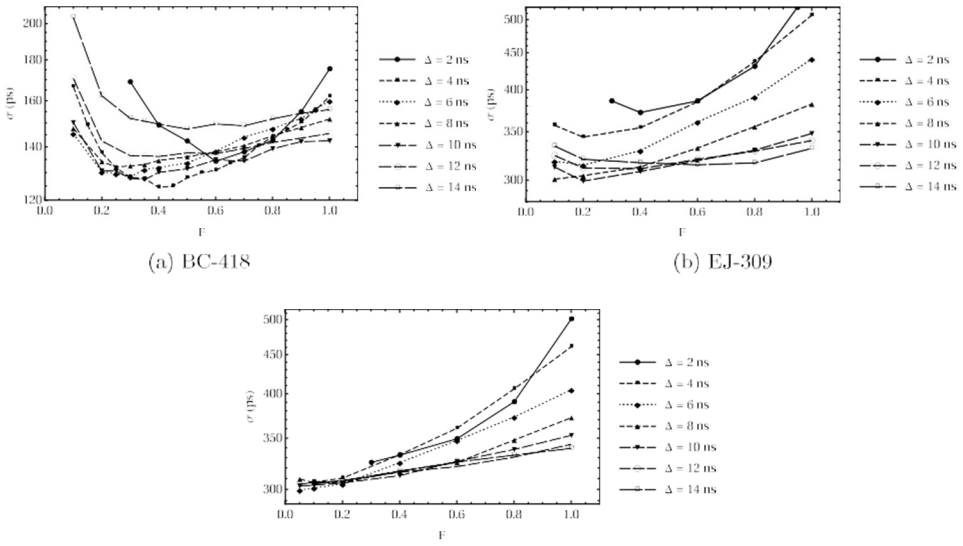

(a) BC-418 (b) EJ-309

(c) EJ-276

Fig. 5. Optimize post-processing parameters □ and □ for each scintillator pair.

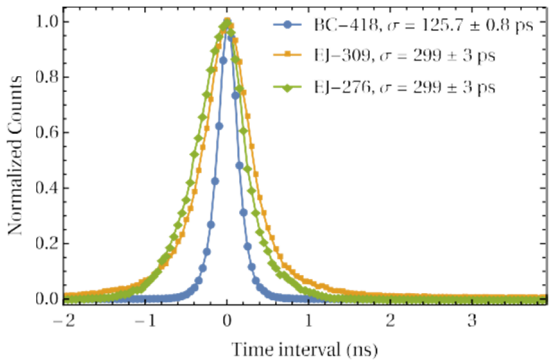

Fig. 6. Optimized time resolution of each scintillator pair.

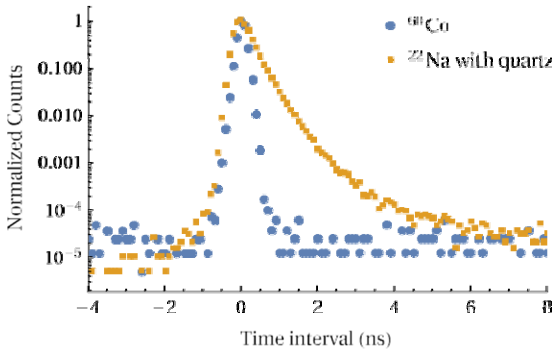

Fig. 7. The ^{60}Co spectrum and the positron lifetime spectrum in single-crystal quartz, measured with BC-418 scintillators.

Table 3
Lifetimes and intensities of the three positron lifetime components.

	□1 (ps)	□2 (ps)	□3 (ns)	□1 (%)	□2 (%)	□3 (%)
Experiment	161 ± 4	343 ± 12	1.34 ± 0.05	53 ± 4	45 ± 4	1.6 ± 0.6
Reference [3,6]	156 ± 4	329 ± 2	1.50 ± 0.03	37.2 ± 0.5	57.5 ± 0.4	5.3 ± 0.2

4. Discussion and conclusions

In this paper we describe the application of fast digitizers and algorithms to measure the positron annihilation lifetime spectra in single-crystal quartz. We found that the positron lifetimes in quartz were 161 ± 4 ps, 343 ± 12 ps and 1.34 ± 0.05 ns, in good agreement with literature values [3,6]. Timing resolution is crucial in PALS measurements as well as in many other applications, such as nuclear medicine and radiation imaging. We have developed algorithms to determine the onset time of pulses and optimize the timing resolution. We reduced the skewness of the time interval distribution by pulse interpolation and found the best time resolution by optimizing the pulse amplitude fraction □ and time delay □. We found □ to be the most relevant post-processing parameter in reducing the actual FWHM. We found an optimum □ factor of 0.4, 0.2 for the two investigated

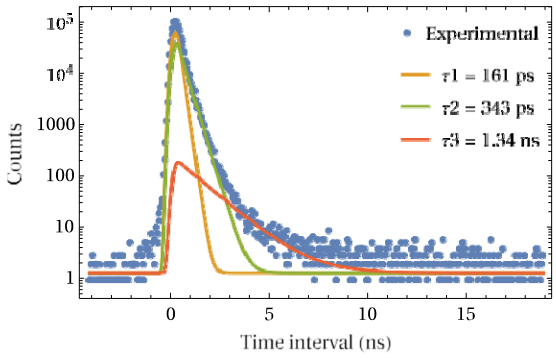

Fig. 8. Fit the PALS spectrum of the single-crystal quartz sample.

scintillators, BC-418 and EJ-309, respectively. The EJ-276 scintillators showed a decreasing FWHM with the □ factor. Therefore, we selected a small □ of 0.05, above the baseline noise. We compared the time resolution of the three different scintillators and found that the proposed interpolation-based approach coupled with a CFD algorithm yielded the best time resolution of 198.3 ± 0.8 ps with BC-418 scintillator that compares well with 208.5 ± 1.1 ps reported by Ralston et al. [19]. We also tested a leading edge timing algorithm, where we calculated the pulse onset as the time when the sampled value exceeds a fixed fraction of pulse height. The CFD-based method yielded a 7-ps-smaller FWHM, showing a slightly better timing resolution compared to the leading edge one. We will use the optimized experimental setup to analyze vacancies and damages created in radiation detectors irradiated at high fluence rates.

Acknowledgments

This work was funded in-part by the Nuclear Regulatory Commission, United States award number 31310018K0002.

References

[1] W. Brandt, S. Berko, W.W. Walker, Positronium decay in molecular substances, Phys. Rev. 120 (4) (1960) 1289, http://dx.doi.org/10.1103/PhysRev.120.1289.

[2] D.W. Gidley, A. Rich, E. Sweetman, D. West, New precision measurements of the decay rates of singlet and triplet positronium, Phys. Rev. Lett. 49 (8) (1982) 525, http://dx.doi.org/10.1103/PhysRevLett.49.525.

[3] H. Saito, T. Hyodo, Direct measurement of the parapositronium lifetime in □- s i o 2, Phys. Rev. Lett. 90 (19) (2003) 193401, http://dx.doi.org/10.1103/PhysRevLett.90.193401.

[4] J. Kansy, K. Mroczka, J. Dutkiewicz, PALS determination of defect density within friction stir welded joints of aluminium alloys, J. Phys.: Conf. Ser. 265 (1) (2011) 012010, http://dx.doi.org/10.1088/1742-6596/265/1/012010.

[5] D.W. Gidley, W.E. Frieze, T.L. Dull, A.F. Yee, E.T. Ryan, H.-M. Ho, Positronium annihilation in mesoporous thin films, Phys. Rev. B 60 (8) (1999) R5157, http://dx.doi.org/10.1103/PhysRevB.60.R5157.

[6] J.D. Van Horn, F. Wu, G. Corsiglia, Y.C. Jean, Asymmetric positron interactions with chiral quartz crystals? in: Defect and Diffusion Forum, Vol. 373, Trans Tech Publ, 2016, pp. 221–226, http://dx.doi.org/10.4028/www.scientific.net/DDF.373.221.

[7] C.H. Hodges, B.T.A. McKee, W. Triftshäuser, A.T. Stewart, Umklapp annihilation of positronium in crystals, Can. J. Phys. 50 (2) (1972) 103–109, http://dx.doi.org/10.1139/p72-019.

[8] M. Jardin, M. Lambrecht, A. Rempel, Y. Nagai, E. Van Walle, A. Almazouzi, Digital positron lifetime spectrometer for measurements of radioactive materials, Nucl. Instrum. Methods Phys. Res. A 568 (2) (2006) 716–722, http://dx.doi.org/10.1016/j.nima.2006.08.087.

[9] K. Rytsölä, J. Nissilä, J. Kokkonen, A. Laakso, R. Aavikko, K. Saarinen, Digital measurement of positron lifetime, Appl. Surf. Sci. 194 (1–4) (2002) 260–263, http://dx.doi.org/10.1016/S0169-4332(02)00128-9.

[10] F. Bečvář, J. Čížek, I. Prochazka, High-resolution positron lifetime measurement using ultra fast digitizers acqiris DC211, Appl. Surf. Sci. 255 (1) (2008) 111–114, http://dx.doi.org/10.1016/j.apsusc.2008.05.184.

[11] CAEN S.pA., CoMPASS Multiparametric DAQ software for physics applications.

[12] W.C. Kaiser, J.A.M. De Villiers, Relative light output evaluation of different commercial plastic scintillators, IEEE Trans. Nucl. Sci. 11 (3) (1964) 29–37, http://dx.doi.org/10.1109/TNS.1964.4323402.

[13] M. Taiuti, P. Rossi, R. Morandotti, M. Anghinolfi, H. Avakian, M. Battaglieri, N. Bianchi, P. Corvisiero, E. DeSanctis, V. Giourjian, et al., Measurement of the response of long plastic scintillator bars for the large angle electromagnetic shower calorimeter for CLAS, Nucl. Instrum. Methods Phys. Res. A 370 (2–3) (1996) 429–434, http://dx.doi.org/10.1016/0168-9002(95)00848-9.

[14] C.E. Shannon, Communication in the presence of noise, Proc. IEEE 86 (2) (1998) 447–457, http://dx.doi.org/10.1109/JPROC.1998.659497.

[15] W.K. Warburton, W. Hennig, New algorithms for improved digital pulse arrival timing with Sub-GSps ADCs, IEEE Trans. Nucl. Sci. 64 (12) (2017) 2938–2950, http://dx.doi.org/10.1109/TNS.2017.2766074.

[16] W.M. Steinberger, M.L. Ruch, A. Di-Fulvio, S.D. Clarke, S.A. Pozzi, Timing performance of organic scintillators coupled to silicon photomultipliers, Nucl. Instrum. Methods Phys. Res. A 922 (2019) 185–192, http://dx.doi.org/10.1016/j.nima.2018.11.099.

[17] J. Kansy, D. Giebel, Study of defect structure with new software for numerical analysis of PAL spectra, J. Phys.: Conf. Ser. 265 (1) (2011) 012030, http://dx.doi.org/10.1088/1742-6596/265/1/012030.

[18] M.L. Chithambo, P. Sane, F. Tuomisto, Positron and luminescence lifetimes in annealed synthetic quartz, Radiat. Meas. 46 (3) (2011) 310–318, http://dx.doi.org/10.1016/j.radmeas.2010.12.003.

[19] J.P. Ralston, Design and Performance Analysis of an Ultra-Fast Digital Positron Annihilation Lifetime Spectrometer (Master's thesis), The Ohio State University, 2013.